forests

MDPI

Article

Smoke Injection Heights from Forest and Grassland Fires in Southwest China Observed by CALIPSO

Wenjia Wang [1], Qixing Zhang [1,*], Ranran Zhao [1], Jie Luo [2] and Yongming Zhang [1]

[1] State Key Laboratory of Fire Science, University of Science and Technology of China, Hefei 230026, China; wwjia@mail.ustc.edu.cn (W.W.); ranz2@mail.ustc.edu.cn (R.Z.); zhangym@ustc.edu.cn (Y.Z.)
[2] State Environment Protection Key Laboratory of Satellite Remote Sensing, Aerospace Information Research Institute, Chinese Academy of Sciences, Beijing 100101, China; ajybfq@mail.ustc.edu.cn
* Correspondence: qixing@ustc.edu.cn; Tel.: +86-551-6360-0770

Abstract: Smoke injection height (SIH) determines the distance and direction of smoke transport, thus impacting the atmospheric environment. In this study, we used Cloud-Aerosol Lidar and Infrared Pathfinder Satellite Observations data coupled with Moderate Resolution Imaging Spectroradiometer (MODIS) data and the Hybrid Single-Particle Lagrangian Integrated Trajectory model to derive the SIH values during the peak forest and grassland fire seasons from 2012 to 2017 in Southwest China. The results suggest that the SIH values ranged from 2500 m to 2890 m. An analysis of the dependence of SIH on fire characteristics revealed no obvious correlation between SIH and fire radiative power (FRP) because other factors in addition to FRP have an important impact on SIH. Moreover, MODIS FRP data has a drawback in representing the energy released by real fires, also leading to this result. The topographic variables of forest and grassland fires in Southwest China are very different. Complex topography affects SIH by affecting fire intensity and interactions with wind. A comparison of the SIHs with boundary layer height reveals that 75% of the SIHs are above the boundary layer. Compared with other areas, a higher percentage of free troposphere injection occurs in Southwest China, indicating that smoke can cause air pollution over large ranges. Our work provides a better understanding of the transport and vertical distribution of smoke in Southwest China.

Keywords: forest and grassland fires; smoke injection height; Cloud-Aerosol Lidar and Infrared Pathfinder Satellite Observations (CALIPSO); Moderate Resolution Imaging Spectroradiometer (MODIS); Hybrid Single-Particle Lagrangian Integrated Trajectory (HYSPLIT) model; Southwest China

check for updates

Citation: Wang, W.; Zhang, Q.; Zhao, R.; Luo, J.; Zhang, Y. Smoke Injection Heights from Forest and Grassland Fires in Southwest China Observed by CALIPSO. *Forests* **2022**, *13*, 390. https://doi.org/10.3390/f13030390

Academic Editor: Paul-Antoine Santoni

Received: 8 February 2022
Accepted: 25 February 2022
Published: 27 February 2022

Publisher's Note: MDPI stays neutral with regard to jurisdictional claims in published maps and institutional affiliations.

Copyright: © 2022 by the authors. Licensee MDPI, Basel, Switzerland. This article is an open access article distributed under the terms and conditions of the Creative Commons Attribution (CC BY) license (https://creativecommons.org/licenses/by/4.0/).

1. Introduction

The smoke released from forest and grassland fires consists of a variety of trace gases and particulate matter. Smoke from forest and grassland fires in the air can have significant impacts in terms of air quality degradation, causing health and safety problems for vegetation and animals, including humans, blocking the transmission of solar radiation, and affecting the climate [1,2]. As a typical characteristic of smoke, the smoke injection height (SIH) is a crucial driver of smoke transport and environmental pollution. In addition, SIH is a key input to most atmospheric models that simulate atmospheric composition or pollutant transport and include wildfire emissions [3,4]. Amiridis et al. [5] found that smoke can be confined to the boundary layer or reach the free atmosphere, thereby having a wider impact after the initial smoke injection stage. The vertical profile of smoke and its injection height can determine whether the fire has localized or widespread impacts. Therefore, quantifying SIH is of great importance for understanding the transport and vertical distribution of forest and grassland fire emissions.

Paugam et al. [4] used a review study to estimate wildfire SIH within large-scale atmospheric chemical transport models. To obtain the SIH from wildfires, many studies [6,7] have established mathematical models and simulated SIH by inputting multiple

relevant parameters, such as fire size, fire radiation power, and atmospheric conditions. Most plume models are complicated, with many input parameters and high computational requirements [8]. In addition to model calculations, Liu et al. [9] used a ceilometer to measure the SIHs from prescribed fires in the southeastern United States (US). Mardi et al. [10] used vertical aircraft sampling to obtain the SIH from biomass burning in the vicinity of the California coast. With the widespread application of satellite remote sensing technology [5,11–15], satellite observations have been commonly used to determine SIH. Satellite observation methods are more convenient for obtaining a wider range of data than ground or aircraft experimental measurements. The Cloud-Aerosol Lidar with Orthogonal Polarization (CALIOP) aboard the Cloud-Aerosol Lidar and Infrared Pathfinder Satellite Observations (CALIPSO) satellite and the Multiangle Imaging SpectroRadiometer (MISR) aboard the US National Aeronautics and Space Administration (NASA) Terra satellite are sensors that have been widely used to retrieve the SIH of wildfires [11,12,14,16]. Kahn et al. [12] suggested that CALIOP and MISR have different advantages in plume observation. CALIPSO data can provide vertical profiles of smoke aerosols, identify thin optical plumes, and capture night plumes. The MISR has a wider orbit and wider detection range for obtaining complete smoke plumes [4,5,13]. Although some studies [12,17] have suggested that the two data sets can be complementary, due to different data acquisition and processing methods [16], the existing studies utilized only one of the two sensors in a single study area.

Previous studies have used CALIPSO products to obtain the SIH and vertical distribution of smoke from wildfires. For example, Yu et al. [18] used CALIPSO data to obtain the SIH and smoke aerosol optical parameter profiles from a wildfire in western Canada on August 12, 2017. Yao et al. [19] used CALIPSO observation data as training data to construct a random forest model to predict the minimum height of smoke from forest fires in the atmosphere. In addition, CALIPSO data were used to statistically analyse the SIHs in wildfire seasons in different regions. Amiridis et al. [5] used CALIPSO data to study the SIHs of summer agricultural fires in southern Russia and Eastern Europe from 2006 to 2008. Gonzalez-Alonso et al. [16] provided an assessment of the SIH distribution in the Amazon burning season from July to November 2006 to 2012 based on CALIPSO data.

Val Martin et al. [14] analysed global wildfire SIHs and found that SIHs have great differences and uncertainties in different regions. Therefore, it is necessary to evaluate and analyse SIHs on a regional scale. Liao et al. [20] proposed that Southwest China is one of the most topographically complex regions in the world. This region is facing varying degrees of air pollution problems caused by local emissions and atmospheric transport of aerosols from surrounding areas. In recent years, increasing attention has been given to the study of fire emissions in Southwest China. For example, Zhu er al. [21] studied the impact of biomass combustion plumes from East and Southeast Asia on Southwest China through smoke transport, but they did not discuss local fire smoke in Southwest China. Zhao et al. [22] simulated the distribution of particulate matter with aerodynamic diameters less than 2.5 μm ($PM_{2.5}$) produced by wildfires to evaluate the impact of regional fire smoke on air quality. They also pointed out that wildfire emissions in Southwest China may affect local densely populated areas. It is well known that forest and grassland fires occur frequently in Southwest China. However, study of the transport and vertical distribution of smoke from forest and grassland fires in Southwest China is still limited.

In this work, Moderate Resolution Imaging Spectroradiometer (MODIS) data and the Hybrid Single-Particle Lagrangian Integrated Trajectory (HYSPLIT) model are coupled with CALIPSO data to establish SIH data groups during the peak season of forest and grassland fires from 2012 to 2017 in Southwest China. To the best of our knowledge, this study shows for the first time the SIH temporal and spatial distribution on a regional scale in China. The obtained data groups provided new regional data for the global wildfire SIH database. The variation in the SIHs of forest and grassland fires in Southwest China was statistically analysed. We further examined the dependence of SIH on fire radiative power (FRP) and topography to explore the factors that may affect SIHs in Southwest

China. Moreover, SIH in relation to boundary layer height (BLH) is also discussed. It is helpful to understand whether the smoke of forest and grassland fires in Southwest China cause smoke transport and air pollution over large ranges.

2. Data and Methods

2.1. Study Area

In this work, Southwest China refers specifically to Xizang Province, Yunnan Province, Chongqing Province, Sichuan Province, and Guizhou Province, which cover a range of 21°08′ N–36°29′ N, 78°17′ E–110°11′ E (Figure 1). Southwest China is the second largest natural forest region in China. The terrain is rather complex and undulating in this region, covering some areas of the Yunnan–Guizhou Plateau, Sichuan Basin, and the Qinghai–Tibetan Plateau. The climate is diverse in this region, including a tropical monsoon climate, subtropical monsoon climate, and plateau alpine climate [23,24]. Due to the warm climate and abundant vegetation resources, this area experiences some of the highest frequencies of forest fires in China [25]. In addition, the specific geographical location, topography, climate, and distribution of forest resources lead to the uniqueness of forest and grassland fires in Southwest China, which are characterized by a low fire intensity but high frequency. Forest and grassland fires in Southwest China mainly occur from November to May of the next year [26,27]. Statistical research shows that the three months with the highest number of fires are February to April [22,27].

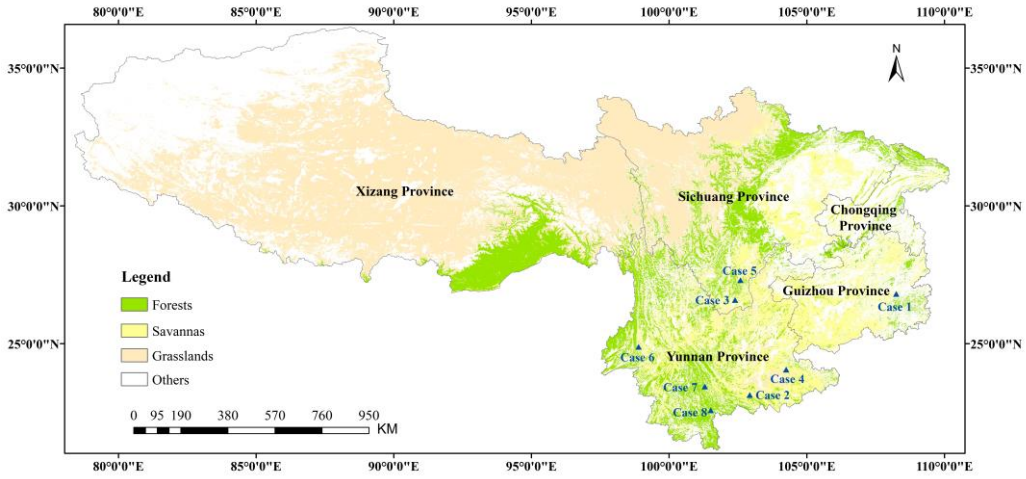


Figure 1. Overview of the study area and the forest and grassland distribution. The eight captured plumes (blue triangles) by CALIOP and corresponding fire case numbers are labelled.

2.2. Data Source

2.2.1. MODIS Data

To identify the areas affected by wildfires in Southwest China, Near Real-Time (NRT) MODIS data were used, which were obtained from the Fire Information for Resource Management System (FIRMS). This system provides daily information on active fires, which includes the locations, times, and FRP values of hotspots. FRP data are always used as indications of fire intensity at the time of observation and are key parameters in the MODIS fire product [28]. The FRP data from MODIS can therefore provide a quantitative assessment of the intensity of global wildfires [29]. A hotspot from MODIS represents the centre of a 1 km pixel that contains one or more fires within the pixel [30]. However, hot fires have a very distinct signature even when they cover a fraction of a MODIS pixel due to the very nonlinear characteristic of the Planck function [11]. Therefore, the active fire product has a confidence level to guarantee the quality of the data. In this study, we used active fire data with a high confidence level (confidence value $\geq$ 75).

The Collection 6 MODIS land cover product (MCD12Q1) [31] provides global land cover information to determine the type of land cover associated with each hotspot. The data were obtained from the NASA Land Process Distributed Active Archive Center with a 500 m × 500 m spatial resolution and yearly temporal resolution. The MCD12Q1 product provides six different classification schemes for different science communities [32]. The University of Maryland classification (UMD) was used for the land cover classification legends in this work. The vegetation subclass in the legends was divided into two categories as forest and grassland.

2.2.2. CALIPSO Data

The CALIOP instrument operates onboard the CALIPSO satellite with two-wavelength polarization lidar (532 and 1064 nm). It can collect backscatter and depolarization data to probe the vertical structure and properties of global clouds and aerosols [33]. The CALIPSO data products provide a characterization of the aerosol type based on algorithms by using integrated attenuated backscatter measurements and volume depolarization ratio measurements, as well as surface type and layer altitude [34]. The latest CALIPSO data products are available from the Langley Atmospheric Science Data Center. In this study, the CALIPSO Vertical Feature Mask (VFM V4-20) product [35] was used. The product provides the vertical profiles and locations of smoke aerosols, which were used to derive the altitude and thickness of the smoke layer from a fire in the atmosphere. The smoke injection altitude was obtained by extracting the altitude data from the highest elevated smoke data block from the aerosol subtype data block in the VFM product. The smoke altitude from CALIPSO is the smoke height based on sea level. In this study, SIH is the smoke height based on ground level. Therefore, we used the smoke injection altitude to subtract the elevation of the land surface and obtained the SIH. We obtained the elevation of the land surface from the GTOPO30 digital elevation map (DEM) for the horizontal distance spanned by the averaged profile, which was included in the individual data fields reported in the CALIPSO cloud and aerosol profile products. Figure 2 shows an example of deriving the SIH from the VFM product over Southwest China on 29 April 2015.

2.2.3. HYSPLIT

HYSPLIT, developed by the National Oceanic and Atmospheric Administration (NOAA)'s Air Resources Laboratory, is one of the most widely used models for atmospheric trajectory and dispersion calculations [36]. It has many applications, including tracking and forecasting the release of wildfire smoke [37]. In this study, the position and time of the smoke derived from CALIOP were inputted into the model and then a backward 24 h trajectory was run. The backward trajectory plots can be useful in determining the hotspots of the upwind source area that may affect the fire plumes captured at the starting location. When the hotspot spatiotemporal information matches the smoke and only one group of hotspots on the backward trajectory is satisfied as the smoke source, the smoke is recorded as produced by a single fire event. Therefore, the trajectory was used to match the corresponding hotspots and smoke in this study. The 24 h backward trajectory connects the smoke and active fire sources, ensuring that the captured smoke was near the fire source and that no other fire events affected the captured smoke at the same time. These data processing methods ensured that the smoke was injected into the atmosphere near the fire source. Mardi et al. [10] proposed that linking smoke to the active fire is helpful in correctly evaluating SIH.

2.3. SIH Data Groups

Although CALIPSO can capture smoke aerosols, it rarely passes directly above the fire source [17]. The smoke observed by CALIPSO may be the joint effect of fires in different times and places. Therefore, it is difficult to exclude the impact of relevant fires on the observed smoke, which could lead to great errors. Soja et al. [37] proposed using HYSPLIT, which provides the backward trajectory to match the smoke and fire, based on the data

processing of CALIPSO and MODIS. In this study, the matching criterion of smoke to hotspots was modified based on the method proposed by Soja et al. [37]. We believed that a higher confidence value of hotspots should be used to ensure the accuracy of MODIS observation of hotspots. In addition, we focused on excluding observed smoke affected by multiple fires. The method of establishing the SIH data group is shown in Figure 3.

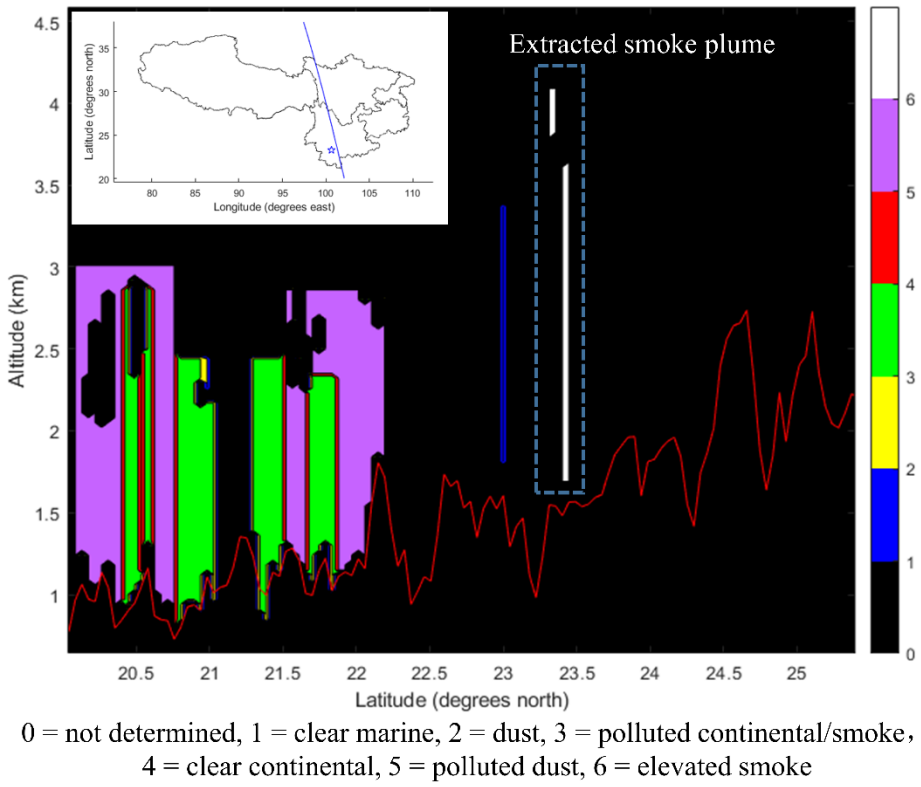


Figure 2. CALIPSO swath and aerosol vertical feature mask of the fire over Southwest China on 29 April 2015. The blue line crossing from south to north is the CALIOP track. The blue star is the location of the fire. The blue dashed box marks the smoke of the fire case captured by CALIPSO. The red line represents the surface elevation below smoke.

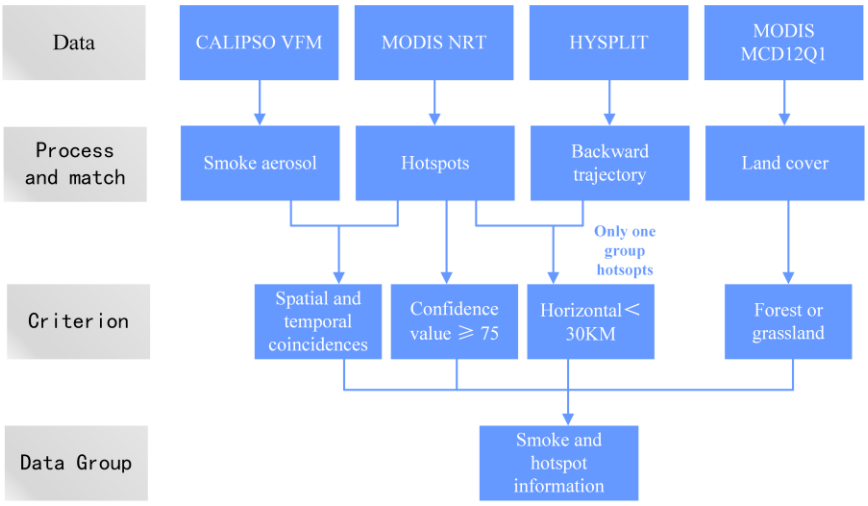


Figure 3. Method of establishing the SIH data groups.

As shown in Figure 3, the data information was processed and matched to identify the fire source of CALIPSO captured smoke. First, a spatial and temporal coincidence of

the smoke and hotspots was identified based on the CALIPSO swath path and hotspot distribution. Next, the time and location of smoke were derived from the CALIPSO aerosol feature mask, and HYSPLIT ran backward in three-dimensional space and time until coincidences were identified with MODIS hotspot locations. It was assumed that the smoke came from the detected fire if: (1) there was temporal and spatial coincidence; (2) the hotspot confidence value was greater than or equal to 75; (3) the vegetation type of the hotspot was forest or grassland; and (4) Within 30 km of the horizontal range of the backward trajectory, only one group of hotspots meets the spatial and temporal of the observed smoke. Then, the obtained smoke and hotspot information was recorded as one SIH data group. The data were derived over Southwest China during the peak forest and grassland fire seasons, which were February to April from 2012 to 2017. Finally, according to the above criteria, we obtained eight representative SIH data groups.

3. Results and Discussion

3.1. Fire Cases and the SIH

We numbered the eight data groups of obtained fire cases as 1–8 in order of the fire occurrence time. Figure 1 shows the plume locations in the eight fire cases captured by CALIPSO. The relevant fire information obtained based on MODIS is shown in Table 1. The smoke information obtained by CALIPSO is given in Table 2. The results show that the SIHs ranged from 2500 m to 2890 m above ground level, with a mean value of 2706.5 ± 147.6 m.

Table 1. Eight cases of forest and grassland fires obtained by MODIS.

Case Number	Detection Data (UTC)	Detection Time (UTC)	FRP (MW)	Dominant Land Cover
Case 1	1 April 2012	06:13	22.3	Grassland
Case 2	29 April 2012	06:37	31.5	Grassland
Case 3	11 March 2013	19:10	13.1	Forest
Case 4	12 April 2014	06:32	13.5	Grassland
Case 5	15 April 2014	19:10	12.7	Forest
Case 6	15 March 2015	19:23	22.7	Grassland
Case 7	29 April 2015	06:44	17.6	Forest
Case 8	15 April 2016	06:44	37	Forest

Table 2. Eight cases of forest and grassland fire SIHs derived from CALIOP.

Case Number	Detection Date (UTC)	Detection Time (UTC)	Altitude (m)	SIH (m)
Case 1	1 April 2012	05:43:52	3580	2833
Case 2	29 April 2012	06:11:56	4120	2878
Case 3	11 March 2013	18:56:00	4750	2711
Case 4	12 April 2014	06:04:17	4030	2500
Case 5	15 April 2014	19:00:13	4780	2890
Case 6	15 March 2015	19:09:13	3340	2562
Case 7	29 April 2015	06:18:40	4090	2745
Case 8	15 April 2016	06:16:34	4300	2533

To improve the understanding of smoke emissions from forest and grassland fires in Southwest China, we collated the SIH data for wildfires observed by satellite observations in previous studies and listed them in Table 3. The differences in SIH distributions were nonnegligible since the SIH depended on fire types and fire spatiotemporal distribution in the different study areas. In a statistical study of the SIH of forest and grassland fires, based on the MISR data, Peterson et al. [15] showed that the average plume injection height in North American boreal forest fires was approximately 1.40 km. Gonzalez-Alonso et al. [16] used CALIPSO to observe the Amazon biomass burning SIH and discovered that the average SIH ranged from 2.1 km (tropical forest and savanna) to 2.3 km (grassland).

Compared with their results, the SIH values obtained in this study were high, indicating that forest and grassland fires in Southwest China can produce high SIHs.

Table 3. Comparison of SIHs with previous observations.

Literature Cited	Period	Fire Type	Study Area	Satellite Sensor	SIH	Relationship with BLH
Amiridis et al. [5]	2006–2008 July and August	Agricultural	SW Russia and Eastern Europe	CALIOP	1677 m–5940 m	48.5% injected into the free troposphere
Peterson et al. [15]	2004–2005 May to September	Boreal forest	North American	MISR	0.28 km–5.01 km	21% injected into the free troposphere
Kahn et al. [12]	2004 Summer	Wildfire	Alaska Yukon	MISR	A few hundred metres to 4.5 km	17.6% injected into the free troposphere
Gonzalez-Alonso et al. [16]	2006–2012 July to November	Biomass burning	Amazon	CALIOP	1.8 km–5.8 km	-
This study	2012–2017 February to April	Forest and grassland	Southwest China	CALIOP	2500 m–2890 m	75% injected into the free troposphere

Paugam et al. [4] summarized previous studies and analysed the physical mechanisms and dynamics of smoke. Their study shows that SIH is driven by both the energy released by a fire and the ambient atmospheric conditions. In short, considering the actual situation of a wildfire incident, the SIH varies by geographical location, vegetation type, and season [14]. To explore the main factors affecting the distribution of the SIHs in Southwest China, we analyse and discuss the dependence of smoke plume height on fire characteristics in the following section.

3.2. Dependence of SIH on Fire Characteristics

FRP describes the energy radiated by the fire per unit time, and previous studies have proved that FRP, as a remote sensing parameter, can characterize fire intensity [38]. Similar to previous studies [5,13], FRP values are used in this study to evaluate the effect of fire intensity on SIH. Table 1 presents the FRP data for the captured fire cases. As the hotspots were screened by confidence level, the FRP of a fire in this study is the mean FRP of the hotspots with a confidence value ≥ 75 in the fire. The results show that the FRP value of forest and grassland fires in Southwest China ranges from approximately 12.7–37 MW per hotspot, and the average FRP is approximately 21.3 MW per hotspot. Wooster et al. [29] compared the fire intensity of boreal forests in Russia and North America based on the FRP. In their study, FRP values were considered low when they were no larger than 50 MW. According to this definition, the fire intensity in this study is low. Laurent el al. [39] analysed the relationships between the FRP and fire size of vegetation fires. They also proposed that the average FRP values (~20–30 MW) were at a low to intermediate level. The forest and grassland fires in Southwest China always occur with a high frequency, a small fire area, and a low fire intensity [22]. The FRP data for the captured fire cases are also in accord with the wildfire characteristics in Southwest China.

Disregarding horizontal transport processes and the vertical thermal profile of the lower atmosphere, the main driver of fire smoke would likely be convection by fire heat; therefore, a higher FRP should cause a higher SIH [5]. However, it is difficult to conclude that a higher FRP results in a higher SIH based on these results (Table 1). Amiridis et al. [5] and Val Martin et al. [13] further investigated the relationship between FRP and SIH in their study area. They concluded that although SIH increases with the increase of FRP

values, the fitting correlation is very poor. They also found that the reason for the weak fitting correlation between SIH and FRP is that, in addition to FRP, atmospheric structure has an important effect on SIH.

In addition, the research of Peterson et al. [15] provides another reason for a low FRP and high SIH. Peterson et al. [15] proposed that FRP values are estimates of fire radiative power released over a pixel area, but the thermal buoyancy provided in real fires is related to subpixel fire areas. Based on FRP, they introduced a calculation for fire radiation power in the subpixel region of active combustion. This calculation helps explain some fire cases with low FRP and high SIH values. They also believe that in addition to fire intensity, the influence of meteorological factors on SIH is very important. The influence of meteorology on SIHs in Southwest China will be investigated in future research.

3.3. Topographical Influences on SIH

In previous regional studies [5,9,16], the influence of topographical factors on SIH was often ignored. Linn et al. [40] pointed out that topography is crucial to wildfire behaviour. Southwest China has a complex topography. As important topographic variables affecting fire behaviour, the elevation, slope aspect, and slope data of all fire cases were obtained from GTOPO30 DEM data and are listed in Table 4 [41]. The results showed that there were great differences in the values of topographic variables in each fire case. Since there are few cases of fire in this study, only the relationship between topographic factors and SIH is qualitatively analysed and discussed. One of the reasons why topography affects SIH is that topography can affect fire intensity. Fang et al. [42] pointed out that there is a strong relationship between topography and fire severity. Liu et al. [9] also found that slash-and-burn fires consume more fuel and release more heat compared to fires on fairly flat terrain that produce a higher SIH. Another reason is that topography interacts with wind and affects the flow of fire smoke. In the study by Susan M. O'Neill [2], it was suggested that complex terrain would have a greater impact on producing a higher SIH. The quantitative relationship between topography and SIH in Southwest China will be analysed and studied through the use of more data in future research.

Table 4. Eight cases of forest and grassland fire topographic variables.

Case Number	Slope (°)	Aspect	Elevation
Case 1	0.43	Southeast	575
Case 2	20.65	Northwest	1092
Case 3	4.98	East	2218
Case 4	9.28	South	1017
Case 5	12.39	North	2690
Case 6	15.11	South	1450
Case 7	9.21	Southwest	1384
Case 8	4.07	North	947

3.4. SIH Relative to BLH

The atmospheric boundary layer (BL) plays an important role in many fields [43], and the BLH determines the volume available for the dispersion of pollutants [44]. By comparing the BLH and SIH, we can assess whether smoke from fires cause a widespread impact. To identify the SIH from the studied cases within or above the BL, we compared SIH with BLH (Figure 4). The BLH of each fire case was obtained from the European Centre for Medium-Range Weather Forecasts (ECMWF) with $0.25^\circ \times 0.25^\circ$ (atmosphere) resolution data per hour [45]. The results showed that most of the SIHs were higher than the BLHs. Figure 4 also presents the frequency distribution of the differences between SIH and BLH. The results showed that in the eight cases of fires examined here, 25% of the SIHs were contained within the BL. For the remaining 75% of the cases, smoke was injected directly into the free troposphere. In addition, the smoke reached heights above the boundary layer on the order of 1 km for 12.25% of the cases and between 2 and even 3 km for 62.25% of the

cases. This means that the smoke emitted from most forest and grassland fires in Southwest China can be injected into the free atmosphere, which may result in smoke transport and air pollution over large ranges. However, many researchers have proposed that different types of wildfire smoke tend to remain within the BL [5,12,15,16]. For example, Labonne et al. [11] used CALIPSO data to study hundreds of biomass combustion cases in eight regions of the world. They concluded that although direct injection into the free troposphere for some fires has been reported, most of the biomass combustion plumes were initially limited to the BL. Table 3 summarizes the detailed statistical data of the percentage of smoke above the BL from previous studies. A higher percentage of fires with SIHs into the free atmosphere is observed in Southwest China than in other regions. The percentage of fires with SIHs into the free atmosphere in Southwest China is several times higher than that for other areas (Table 3). However, when Mardi et al. [10] used airborne lidar to measure the SIHs from biomass burning near the coast of California, they also found, unlike other studies [11], that most of the smoke entered the free atmosphere rather than the boundary layer. Based on these results, Mardi et al. [10] proposed that previous studies preferred to link smoke to atmosphere transport rather than active fires [11]. In addition, the MISR observation causes an underestimation of SIH [12,15]. In this study, we attempt to link SIH to the active fire source.

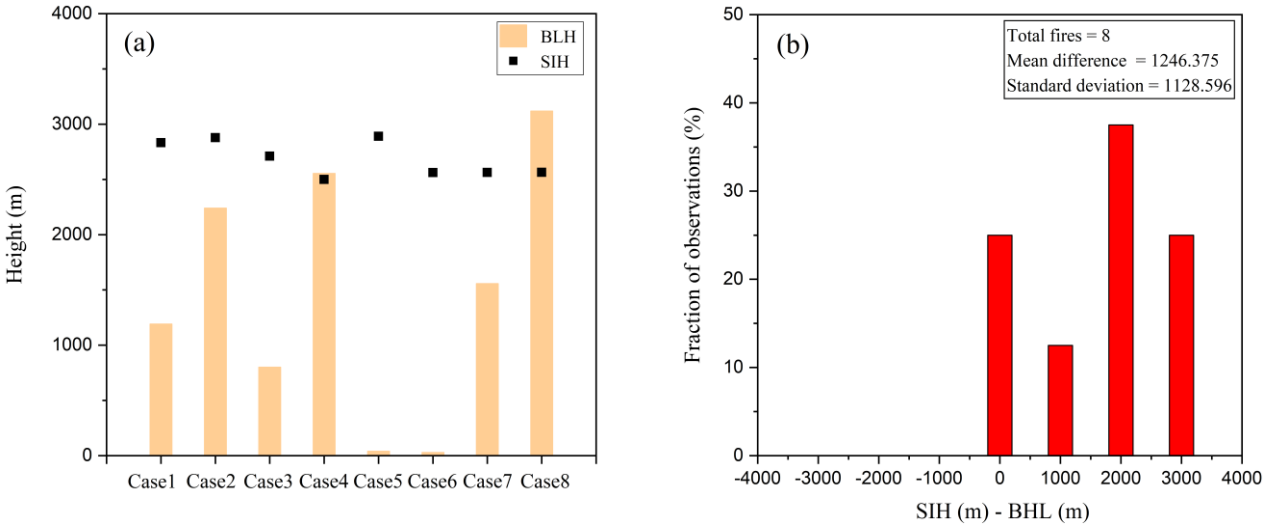


Figure 4. (**a**) Comparison of SIH and BLH. (**b**) Frequency distribution of the differences between SIH and BLH binned in 1000 m height intervals.

There are two other reasons for the high percentage of plumes injected into the free troposphere in Southwest China. One of the reasons may be that the SIH values obtained in this study are high. By analysing the temporal and spatial distribution of BLHs in different regions of China based on years of meteorological data, Zhao et al. [46] showed that a lower BLH was observed in Southwest China due to the relatively lower wind speeds, less sunshine, and higher relative humidity. In addition, in this study, CALIOP captured smoke at approximately 06:00 (14:00 BJT) and 19:00 (03:00 BJT) (Table 2) in the study area. The main factors affecting BLs include surface solar radiation thermal disturbance processes, topographic dynamic disturbance processes, atmospheric boundary layer top entrainment thermal dynamic processes, horizontal and vertical diffusion processes, etc. [47,48]. Therefore, BLHs have significant temporal and spatial variation characteristics. The results from the study by Guo et al. [48] showed that the BLH in Southwest China reaches its peak in the afternoon and is relatively low at night in spring and summer. Figure 5 shows the distribution of BLHs in Southwest China in the afternoon (case 4) and at night (case 5). The results show that the BLH in the afternoon is much higher than that at night in Southwest China. Therefore, we find that fire smoke captured by CALIPSO in the afternoon is more

likely to be trapped in the boundary layer (Table 2). In short, the temporal and spatial distribution of BLHs in Southwest China also accounts for the high percentage of smoke injected into the free atmosphere in this study.

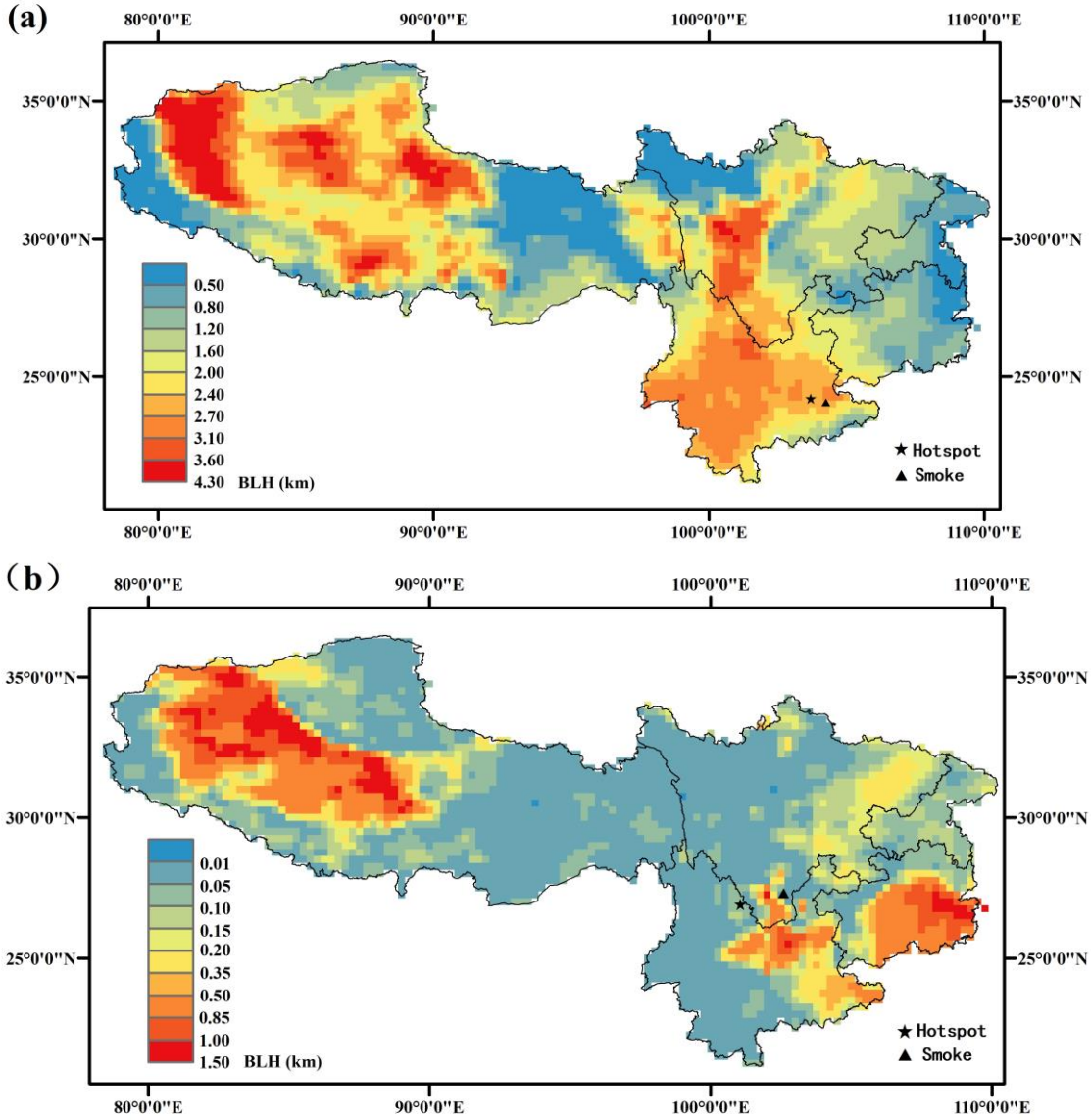


Figure 5. Distribution of the BLHs in Southwest China in (**a**) the afternoon (case 4) and (**b**) at night (case 5).

4. Conclusions

In this study, CALIPSO data were used to derive SIHs during the forest and grassland fire seasons from 2012 to 2017 in Southwest China. The MODIS fire products were coupled with the HYSPLIT model to attribute the identified smoke to fire sources. The SIHs from captured fire cases were analysed to investigate the vertical distribution and transport of smoke from forest and grassland fires. The results suggested that the SIH values ranged from 2500 m to 2890 m above ground level, with a mean value of 2706.5 ± 147.6 m in Southwest China; these values showed little deviation and indicated a high level. Although a higher FRP value means a higher fire intensity, which should cause a higher SIH, the results in this study do not indicate that a higher FRP value leads to a higher SIH because, in addition to FRP, other factors have an important impact on SIH, e.g., meteorological factors. Moreover, MODIS FRP data has a drawback in representing the energy released by real fires within a given fire pixel. The influence of topography on SIH has been ignored in

previous studies. The cases of forest and grassland fires in Southwest China show complex and differentiated topographic variables. Through qualitative analysis, the topography of Southwest China mainly affects SIH by affecting fire intensity and the interaction of fire with wind. A comparison of SIH with BLH reveals that smoke was injected directly into the free troposphere in 75% of the cases examined. Compared with other areas, a significantly higher percentage of smoke was injected into the free troposphere in Southwest China. The results indicated that the smoke emitted from most forest and grassland fires in Southwest China can be injected into the free troposphere, which is likely to result in smoke being transported and air pollution over large ranges. Moreover, through the analysis, the high SIHs and the temporal and spatial variations in the BLH in Southwest China can cause a high percentage of smoke to be injected into the free troposphere.

This work is helping to improve the understanding of the smoke transport and vertical distribution caused by forest and grassland fire emissions in Southwest China. At the same time, the current work also provides new regional data for the global wildfire SIH database.

Author Contributions: Conceptualization, W.W. and Q.Z.; methodology, W.W. and Q.Z.; formal analysis, W.W., R.Z., and J.L.; writing—original draft preparation, W.W. and R.Z; writing—review and editing, all authors; project administration, Q.Z. and Y.Z.; funding acquisition, Q.Z. and Y.Z. All authors have read and agreed to the published version of the manuscript.

Funding: This research was funded by the National Key Research and Development Plan (Grant No. 2020YFC1511600), the National Natural Science Foundation of China (Grant No. 41675024), and Fundamental Research Funds for the Central Universities (Grant No. WK2320000052).

Data Availability Statement: The data presented in this study are available on request from the corresponding author.

Acknowledgments: We thank NASA and CNES for making the CALIPSO data available to the scientific community. The MODIS data and products are distributed by NASA's Land Processes Distributed Active Archive Center. The HYSPLIT is developed by NOAA's Air Resources Laboratory. The ECMWF Boundary Layer Height product is provided by the Copernicus Climate Change Service.

Conflicts of Interest: The authors declare no conflict of interest.

References

1. Andreae, M.O. Biomass burning-Its history, use, and distribution and its impact onenvironmental quality and global climate. In *Global Biomass Burning: Atmospheric, Climatic, and Biospheric Implications*; MIT Press: Cambridge, MA, USA, 1991; pp. 3–21.
2. O'Neill, S.; Urbanski, S.; Goodrick, S.; Larkin, S. Smoke plumes: Emissions and effects. *Fire Manag. Today* **2017**, *75*, 10–15.
3. Colarco, P.R.; Schoeberl, M.R.; Doddridge, B.G.; Marufu, L.T.; Torres, O.; Welton, E.J. Transport of smoke from Canadian forest fires to the surface near Washington, D.C.: Injection height, entrainment, and optical properties. *J. Geophys. Res. Atmos.* **2004**, *109*. [CrossRef]
4. Paugam, R.; Wooster, M.; Freitas, S.; Martin, M.V. A review of approaches to estimate wildfire plume injection height within large-scale atmospheric chemical transport models. *Atmos. Chem. Phys.* **2016**, *16*, 907–925. [CrossRef]
5. Amiridis, V.; Giannakaki, E.; Balis, D.S.; Gerasopoulos, E.; Pytharoulis, I.; Zanis, P.; Kazadzis, S.; Melas, D.; Zerefos, C. Smoke injection heights from agricultural burning in Eastern Europe as seen by CALIPSO. *Atmos. Chem. Phys.* **2010**, *10*, 11567–11576. [CrossRef]
6. Sofiev, M.; Ermakova, T.; Vankevich, R. Evaluation of the smoke-injection height from wild-land fires using remote-sensing data. *Atmos. Chem. Phys.* **2012**, *12*, 1995–2006. [CrossRef]
7. Kukkonen, J.; Nikmo, J.; Sofiev, M.; Riikonen, K.; Petäjä, T.; Virkkula, A.; Levula, J.; Schobesberger, S.; Webber, D.M. Applicability of an integrated plume rise model for the dispersion from wild-land fires. *Geosci. Model Dev.* **2014**, *7*, 2663–2681. [CrossRef]
8. Wang, S.; Cohen, J.B.; Lin, C.; Deng, W. Constraining the relationships between aerosol height, aerosol optical depth and total column trace gas measurements using remote sensing and models. *Atmos. Chem. Phys.* **2020**, *20*, 15401–15426. [CrossRef]
9. Liu, Y.; Goodrick, S.L.; Achtemeier, G.L.; Forbus, K.; Combs, D. Smoke plume height measurement of prescribed burns in the south-eastern United States. *Int. J. Wildland Fire* **2013**, *22*, 130–147. [CrossRef]
10. Mardi, A.H.; Dadashazar, H.; MacDonald, A.B.; Braun, R.A.; Crosbie, E.; Xian, P.; Thorsen, T.J.; Coggon, M.M.; Fenn, M.A.; Ferrare, R.A.; et al. Biomass Burning Plumes in the Vicinity of the California Coast: Airborne Characterization of Physicochemical Properties, Heating Rates, and Spatiotemporal Features. *J. Geophys. Res. Atmos.* **2018**, *123*, 13560–13582. [CrossRef]
11. Labonne, M.; Breon, F.-M.; Chevallier, F. Injection height of biomass burning aerosols as seen from a spaceborne lidar. *Geophys. Res. Lett.* **2007**, *34*. [CrossRef]

12. Kahn, R.A.; Chen, Y.; Nelson, D.L.; Li, Q.; Diner, D.J.; Logan, J.A.; Leung, F.-Y. Wildfire smoke injection heights: Two perspectives from space. *Geophys. Res. Lett.* **2008**, *35*. [CrossRef]
13. Val Martin, M.; Logan, J.A.; Kahn, R.A.; Leung, F.-Y.; Nelson, D.L.; Diner, D.J. Smoke injection heights from fires in North America: Analysis of 5 years of satellite observations. *Atmos. Chem. Phys.* **2010**, *10*, 1491–1510. [CrossRef]
14. Val Martin, M.; Kahn, R.A.; Tosca, M.G. A Global Analysis of Wildfire Smoke Injection Heights Derived from Space-Based Multi-Angle Imaging. *Remote Sens.* **2018**, *10*, 1609. [CrossRef]
15. Peterson, D.; Hyer, E.; Wang, J. Quantifying the potential for high-altitude smoke injection in the North American boreal forest using the standard MODIS fire products and subpixel-based methods. *J. Geophys. Res. Atmos.* **2014**, *119*, 3401–3419. [CrossRef]
16. Gonzalez-Alonso, L.; Martin, M.V.; Kahn, R.A. Biomass-burning smoke heights over the Amazon observed from space. *Atmos. Chem. Phys.* **2019**, *19*, 1685–1702. [CrossRef]
17. Raffuse, S.M.; Craig, K.J.; Larkin, N.K.; Strand, T.T.; Sullivan, D.C.; Wheeler, N.J.M.; Solomon, R. An Evaluation of Modeled Plume Injection Height with Satellite-Derived Observed Plume Height. *Atmosphere* **2012**, *3*, 103–123. [CrossRef]
18. Yu, P.; Toon, O.B.; Bardeen, C.G.; Zhu, Y.; Rosenlof, K.H.; Portmann, R.W.; Thornberry, T.D.; Gao, R.-S.; Davis, S.M.; Wolf, E.T.; et al. Black carbon lofts wildfire smoke high into the stratosphere to form a persistent plume. *Science* **2019**, *365*, 587–590. [CrossRef]
19. Yao, J.; Raffuse, S.M.; Brauer, M.; Williamson, G.J.; Bowman, D.M.; Johnston, F.H.; Henderson, S.B. Predicting the minimum height of forest fire smoke within the atmosphere using machine learning and data from the CALIPSO satellite. *Remote Sens. Environ.* **2018**, *206*, 98–106. [CrossRef]
20. Liao, T.; Gui, K.; Li, Y.; Wang, X.; Sun, Y. Seasonal distribution and vertical structure of different types of aerosols in southwest China observed from CALIOP. *Atmos. Environ.* **2021**, *246*, 118145. [CrossRef]
21. Zhu, J.; Xia, X.; Wang, J.; Zhang, J.; Wiedinmyer, C.; Fisher, J.A.; Keller, C.A. Impact of Southeast Asian smoke on aerosol properties in Southwest China: First comparison of model simulations with satellite and ground observations. *J. Geophys. Res. Atmos.* **2017**, *122*, 3904–3919. [CrossRef]
22. Zhao, F.; Liu, Y.; Shu, L.; Zhang, Q. Wildfire Smoke Transport and Air Quality Impacts in Different Regions of China. *Atmosphere* **2020**, *11*, 941.
23. Tian, X.; Zhao, F.; Shu, L.; Wang, M. Hotspots from satellite monitoring and Forest Fire Weather Index analysis for Southwest China. *For. Res.* **2010**, *23*, 523–529.
24. Xiong, Q.; He, Y.; Li, T.; Yu, L. Spatiotemporal Patterns of Vegetation Coverage and Response to Climatic and Topographic Factors in Growth Season in Southwest China. *Res. Soiland Water Conserv.* **2019**, *26*, 259–266.
25. Tian, X.; Zhao, F.; Shu, L.; Wang, M. Distribution characteristics and the influence factors of forest fires in China. *For. Ecol. Manag.* **2013**, *310*, 460–467. [CrossRef]
26. Zhao, F.; Liu, Y. Atmospheric Circulation Patterns Associated With Wildfires in the Monsoon Regions of China. *Geophys. Res. Lett.* **2019**, *46*, 4873–4882. [CrossRef]
27. Tian, X.-R.; Zhao, F.-J.; Shu, L.-F.; Wang, M.-Y. Changes in forest fire danger for south-western China in the 21st century. *Int. J. Wildland Fire* **2014**, *23*, 185–195. [CrossRef]
28. Kaufman, Y.J.; Ichoku, C.; Giglio, L.; Korontzi, S.; Chu, D.A.; Hao, W.M.; Li, R.-R.; Justice, C.O. Fire and smoke observed from the Earth Observing System MODIS instrument–products, validation, and operational use. *Int. J. Remote Sens.* **2003**, *24*, 1765–1781. [CrossRef]
29. Wooster, M.J.; Zhang, Y.H. Boreal forest fires burn less intensely in Russia than in North America. *Geophys. Res. Lett.* **2004**, *31*. [CrossRef]
30. Giglio, L.; Descloitres, J.; Justice, C.O.; Kaufman, Y.J. An Enhanced Contextual Fire Detection Algorithm for MODIS. *Remote Sens. Environ.* **2003**, *87*, 273–282. [CrossRef]
31. Friedl, M.; Sulla-Menashe, D. *MCD12Q1 MODIS/Terra+Aqua Land Cover Type Yearly L3 Global 500m SIN Grid V006*; NASA EOSDIS Land Processes DAAC: San Diego, CA, USA, 2019.
32. Sulla-Menashe, D.; Gray, J.; Abercrombie, S.P.; Friedl, M.A. Hierarchical mapping of annual global land cover 2001 to present: The MODIS Collection 6 Land Cover product. *Remote Sens. Environ.* **2019**, *222*, 183–194.
33. Vaughan, M.; Young, S.A.; Winker, D.M.; Powell, K.A.; Omar, A.H.; Liu, Z.; Hu, Y.; Hostetler, C.A. Fully automated analysis of space-based lidar data: An overview of the CALIPSO retrieval algorithms and data products. In *Laser Radar Techniques for Atmospheric Sensing*; SPIE: Bellingham, WA, USA, 2004; Volume 5575, pp. 16–30.
34. Omar, A.H.; Winker, D.M.; Vaughan, M.A.; Hu, Y.; Trepte, C.R.; Ferrare, R.A.; Lee, K.-P.; Hostetler, C.A.; Kittaka, C.; Rogers, R.R.; et al. The CALIPSO Automated Aerosol Classification and Lidar Ratio Selection Algorithm. *J. Atmos. Ocean. Technol.* **2009**, *26*, 1994–2014. [CrossRef]
35. Kim, M.-H.; Omar, A.H.; Tackett, J.L.; Vaughan, M.A.; Winker, D.M.; Trepte, C.R.; Hu, Y.; Liu, Z.; Poole, L.R.; Pitts, M.C.; et al. The CALIPSO Version 4 Automated Aerosol Classification and Lidar Ratio Selection Algorithm. *Atmos. Meas. Tech.* **2018**, *11*, 6107–6135. [CrossRef]
36. Stein, A.F.; Draxler, R.R.; Rolph, G.D.; Stunder, B.J.B.; Cohen, M.D.; Ngan, F. NOAA's HYSPLIT Atmospheric Transport and Dispersion Modeling System. *Bull. Am. Meteorol. Soc.* **2015**, *96*, 2059–2077. [CrossRef]
37. Soja, A.J.; Fairlie, T.D.; Westberg, M.D.J.; Pouliot, G. Biomass burning plume injection height using CALIOP, MODIS and the NASA Langley Trajectory Model. In Proceedings of the 2012 International Emission Inventory Conference, Tampa, FL, USA, 13–16 August 2012.

38. Heward, H.; Smith, A.M.S.; Roy, D.P.; Tinkham, W.T.; Hoffman, C.; Morgan, P.; Lannom, K.O. Is burn severity related to fire intensity? Observations from landscape scale remote sensing. *Int. J. Wildland Fire* **2013**, *22*, 910–918. [CrossRef]
39. Laurent, P.; Mouillot, F.; Moreno, M.V.; Yue, C.; Ciais, P. Varying relationships between fire radiative power and fire size at a global scale. *Biogeosciences* **2019**, *16*, 275–288. [CrossRef]
40. Linn, R.; Winterkamp, J.; Edminster, C.; Colman, J.J.; Smith, W.S. Coupled influences of topography and wind on wildland fire behaviour. *Int. J. Wildland Fire* **2007**, *16*, 183–195. [CrossRef]
41. Miliaresis, G.C.; Argialas, D.P. Segmentation of physiographic features from the global digital elevation model/GTOPO30. *Comput. Geosci.* **1999**, *25*, 715–728. [CrossRef]
42. Fang, L.; Yang, J.; Zu, J.; Li, G.; Zhang, J. Quantifying influences and relative importance of fire weather, topography, and vegetation on fire size and fire severity in a Chinese boreal forest landscape. *For. Ecol. Manag.* **2015**, *356*, 2–12. [CrossRef]
43. Garratt, J.R. The Atmospheric Boundary-Layer—Review. *Earth-Sci. Rev.* **1994**, *37*, 89–134. [CrossRef]
44. Seibert, P.; Beyrich, F.; Gryning, S.-E.; Joffre, S.; Rasmussen, A.; Tercier, P. Review and intercomparison of operational methods for the determination of the mixing height. *Atmos. Environ.* **2000**, *34*, 1001–1027. [CrossRef]
45. Hersbach, H.; Bell, B.; Berrisford, P.; Biavati, G.; Horányi, A.; Muñoz Sabater, J.; Nicolas, J.; Peubey, C.; Radu, R.; Rozum, I.; et al. ERA5 hourly data on single levels from 1979 to present. In *Copernicus Climate Change Service (C3S) Climate Data Store (CDS)*; ECMWF: Reading, UK, 2018.
46. Zhao, H.; Che, H.; Xia, X.; Wang, Y.; Wang, H.; Wang, P.; Ma, Y.; Yang, H.; Liu, Y.; Wang, Y.; et al. Climatology of mixing layer height in China based on multi-year meteorological data from 2000 to 2013. *Atmos. Environ.* **2019**, *213*, 90–103. [CrossRef]
47. Che, J.; Zhao, P.; Shi, Q.; Yang, Q. Research progress in atmospheric boundary layer. *Chin. J. Geophys.* **2021**, *64*, 735–751.
48. Guo, J.; Miao, Y.; Zhang, Y.; Liu, H.; Li, Z.; Zhang, W.; He, J.; Lou, M.; Yan, Y.; Bian, L.; et al. The climatology of planetary boundary layer height in China derived from radiosonde and reanalysis data. *Atmos. Chem. Phys.* **2016**, *16*, 13309–13319. [CrossRef]